Inorganic Chemistry

Article

pubs.acs.org/IC

Kinetic Effects of Sulfur Oxidation on Catalytic Nitrile Hydration: Nitrile Hydratase Insights from Bioinspired Ruthenium(II) Complexes

Davinder Kumar, Tho N. Nguyen, and Craig A. Grapperhaus*

Department of Chemistry, University of Louisville, 2320 South Brook Street, Louisville, Kentucky 40292, United States

Supporting Information

ABSTRACT: Kinetic investigations inspired by the metalloenzyme nitrile hydratase were performed on a series of ruthenium(II) complexes to determine the effect of sulfur oxidation on catalytic nitrile hydration. The rate of benzonitrile hydration was quantified as a function of catalyst, nitrile, and water concentrations. Precatalysts L^nRuPPh_3 (n = 1−3; L^1 = 4,7-bis(2′-methyl-2′-mercapto-propyl)-1-thia-4,7-diazacyclononane; L^2 = 4-(2′-methyl-2′-sulfinato-propyl)-7-(2′-methyl-2′-mercapto-propyl)-1-thia-4,7-diazacyclononane; L^3 = 4-(2′-methyl-2′-sulfinatopropyl)-7-(2′-methyl-2′-sulfenato-propyl)-1-thia-4,7-diazacyclononane) were activated by substitution of triphenylphosphine with substrate in hot dimethylformamide solution. Rate measurements are consistent with a dynamic equilibrium between inactive aqua (L^nRu-OH_2) and active nitrile ($L^nRu-NCR$) derivatives with K = 21 ± 1, 9 ± 0.9, and 23 ± 3 for L^1 to L^3, respectively. Subsequent hydration of the $L^nRu-NCR$ intermediate yields the amide product with measured hydration rate constants (k's) of 0.37 ± 0.01, 0.82 ± 0.07, and 1.59 ± 0.12 M^{-1} h^{-1} for L^1 to L^3, respectively. Temperature dependent studies reveal that sulfur oxidation lowers the enthalpic barrier by 27 kJ/mol, but increases the entropic barrier by 65 J/(mol K). Density functional theory (DFT) calculations (B3LYP/LanL2DZ (Ru); 6-31G(d) (all other atoms)) support a nitrile bound catalytic cycle with lowering of the reaction barrier as a consequence of sulfur oxidation through enhanced nitrile binding and attack of the water nucleophile through a highly organized transition state.

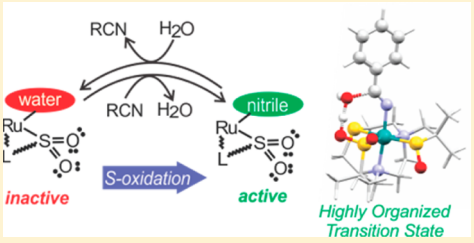

INTRODUCTION

Numerous soil bacteria employ nitrile hydratase (NHase) for the catalytic hydration of nitriles to amides for the initial step in nitrile assimilation.[1−5] It has been well-documented that post-translational sulfur oxidation of cysteine residues at the metal-containing active site is required for catalytic activity in both Co- and Fe-NHases (Figure 1). While several groups have

Figure 1. Co-NHase active site (left) and L^nRuPPh_3 (n = 1−3) (right).

prepared synthetic models of NHase with and without oxidized S-donors,[4,6−17] to date there are no reported functional Fe-based mimics and only four Co-based mimics that catalyze nitrile hydration.[6,9,16,17] *Although there has been much speculation on the role of S-oxygenation in NHase, the lack of functional models with variable sulfur oxidation levels and high activity has prohibited a systematic evaluation of the kinetic effect of S-oxidation on nitrile hydration.* Herein, we report the first such studies employing catalytically active, bioinspired Ru complexes with S-donors in three distinct oxidation states (Figure 1).

Recently, we reported the series of Ru complexes L^nRuPPh_3 (n = 1−3) with variable S-oxidation levels inspired by the active site of NHase.[18−20] Using Ru(II) as a surrogate low-spin d^6 metal, our complexes reproduce key features of the N_2S_3 environment at the active site of Fe- and Co-NHase[2,3,5] including the cofacial positioning of the substrate binding site with sulfenato (RSO^-) and sulfinato (RSO_2^-) donors.[21] In our initial report, we showed the precatalysts L^nRuPPh_3 (n = 1−3) display NHase activity with high turnover numbers (TONs) relative to other NHase mimics.[22] Notably, these are the only structurally characterized, functional mimics of NHase capable of addressing the kinetic effects of S-oxidation on catalytic activity. Preliminary studies suggested that S-oxidation enhances hydration at low nitrile to water ratios and reduces product inhibition.[22]

RESULTS AND DISCUSSION

Kinetic Studies. Although previous results under biphasic conditions indicated that sulfur oxidation enhances nitrile hydration at lower nitrile/water ratios, additional insights into the effect of S-oxidation require the detailed kinetic investigations described in the present study. *Reactions were conducted in dimethylformamide (DMF) to allow complete mixing of the benzonitrile and water substrates with the precatalysts as a homogeneous solution.* Preliminary studies under these con-

Received: July 15, 2014
Published: November 14, 2014

   dx.doi.org/10.1021/ic501695n | Inorg. Chem. 2014, 53, 12372−12377

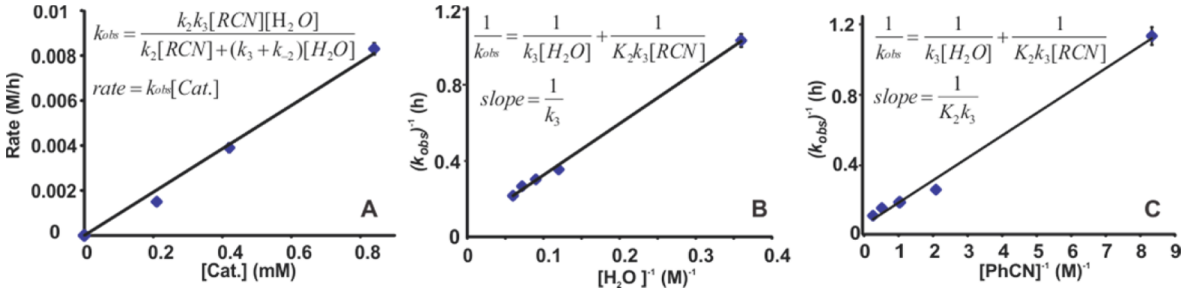

Figure 2. Kinetic plots for [L^1RuPPh_3]: (A) hydration rate (M/h) vs catalyst concentration over a range 0.21−0.84 mM used to determine k_{obs}; (B) $1/k_{obs}$ vs $1/[H_2O]$ where k_{obs} = rate/[L^1RuPPh_3] at constant [PhCN] with [H_2O] from 2.8 to 17 M used to evaluate the product k_3; and (C) $1/k_{obs}$ vs 1/[PhCN] where k_{obs} = rate/[L^1RuPPh_3] at constant [H_2O] with [PhCN] from 0.12 to 4.0 M used to evaluate the product K_2k_3.

ditions revealed a maximum turnover frequency (TOF) of 11 and 62 h^{-1} for precatalysts L^1RuPPh_3 and L^3RuPPh_3, respectively. As in the prior study, high reaction temperatures (368−398 K) were maintained to ensure complete dissociation of the triphenylphosphine donor from the precatalysts L^nRuPPh_3. Aliquots were removed at timed intervals for analysis by GC−MS with the addition of *p*-toluamide as internal standard. Additional experimental details are provided under the Experimental Section.

Experimental kinetic data is consistent with the nitrile-bound hydration mechanism outlined in eqs 1−4. The first step involves activation of the precatalyst via PPh_3 dissociation to form the aqua complex $LRuOH_2$ (eq 1). Under the reaction conditions, PPh_3 dissociation is complete ($k_1 \gg k_{-1}$) such that $[LRuPPh_3]_{initial} = [LRuOH_2]_{initial}$. The aqua complex is in equilibrium ($K_2 = k_2/k_{-2}$) with the nitrile complex LRuNCR (eq 2). The kinetic data could be interpreted with either the $LRuOH_2$ or LRuNCR species as the catalytically competent intermediate. However, since the former is disfavored on the basis of density functional theory (DFT) calculations (*vida infra*), we report the data based on a nitrile bound route. Hydration of LRuNCR via an activated water molecule (eq 3) yields the product complex $LRuNH_2C(O)R$. Under the conditions of low turnover ($[NH_2C(O)R \ll [H_2O]$), the amide is quickly and effectively substituted by H_2O to complete the cycle (eq 4). The rate law for the proposed mechanism (eq 5) was derived assuming steady-state conditions. Consistent with this mechanism, the reaction is first-order with respect to the L^1RuPPh_3 precatalyst (Figure 2A).

$$LRuPPh_3 + H_2O \underset{k_{-1}}{\overset{k_1}{\rightleftarrows}} LRuOH_2 + PPh_3 \quad (1)$$

$$LRuOH_2 + RCN \underset{k_{-2}}{\overset{k_2}{\rightleftarrows}} LRuNCR + H_2O \quad (2)$$

$$LRuNCR + H_2O \overset{k_3}{\rightarrow} LRuNH_2C(O)R \quad (3)$$

$$LRuNH_2C(O)R + H_2O \overset{\text{fast}}{\longrightarrow} LRuOH_2 + RC(O)NH_2 \quad (4)$$

$$\text{rate} = \frac{k_2k_3[LRuPPh_3][RCN][H_2O]}{k_2[RCN] + (k_3 + k_{-2})[H_2O]} \quad (5)$$

$$\frac{1}{k_{obs}} = \frac{1}{k_3[H_2O]} + \frac{1}{K_2k_3[RCN]} \quad (6)$$

Both the water and nitrile substrates display saturation kinetics for L^1RuPPh_3 and L^2RuPPh_3. For L^3RuPPh_3 saturation behavior is observed with nitrile, while a linear dependence is maintained over the entire water concentration range tested indicative of relatively fast nitrile binding. A thermodynamic preference for nitrile is also observed by DFT results (gas and DMF phase) that show that nitrile binding is favored over water by 11.6 and 19.5 kJ/mol in gas and DMF phase, respectively. The hydration rate constant k_3 and nitrile binding equilibrium constant K_2 are determined from the slopes of double reciprocal plots of k_{obs} versus water (Figure 2B) and nitrile concentrations (Figure 2C) (with the exception of k_3 for L^3RuPPh_3 which is calculated from the normal plot of k_{obs} vs water concentration) according to eq 6. Numerical results are summarized in Table 1. Each experiment was performed in triplicate. Reported benzamide concentrations are the average of the three trials with error bar denoting the standard deviation. The errors in the measurement of rate and k_{obs} are determined from a least-squares-fit using the LINEST function in Excel. For $1/k_{obs}$, the error is calculated using the law of error of propagation. The same technique is used for the calculation of error in K_2 and k_3.

Table 1. Water/Nitrile Equilibrium Constant (K_2) and Hydration Rate Constant (k_3) for L^nRuPPh_3 (n = 1−3) in DMF Solvent at 398 K

precatalyst	$K_2 = k_2/k_{-2}$	k_3 (M^{-1} h^{-1})
L^1RuPPh_3	21 ± 1	0.37 ± 0.01
L^2RuPPh_3	9.0 ± 0.9	0.82 ± 0.07
L^3RuPPh_3	23 ± 3	1.59 ± 0.12

Interestingly, S-oxidation results in a steady increase in the hydration rate constant k_3. The sulfinate complex L^2RuNCR hydrates at twice the rate of the thiolate precursor. Further oxidation to the mixed sulfenate/sulfinate L^3RuNCR again results in a doubling of the hydration rate constant. To our knowledge, these are the first kinetic studies to show an increase in the nitrile hydration rate constant upon oxidation of sulfur donors. The influence of S-oxidation on the nitrile/water binding preference (K_2) is less intuitive. All complexes display a small preference for nitrile coordination although K_2 drops by a factor of 2 upon oxidation of L^1RuPPh_3 to L^2RuPPh_3 before rebounding to its original value upon further oxidation to L^3RuPPh_3. Density functional theory calculations (*vida infra*) reproduce the unexpected, alternating behavior of nitrile binding affinity.

Hydration reactions employing deuterium oxide display a secondary kinetic isotope effect for all three precatalysts with KIE (k_H/k_D) values of 1.08 ± 0.05, 0.96 ± 0.04, and 1.32 ± 0.21 for L^1, L^2, and L^3, respectively. This suggests that O−H

dx.doi.org/10.1021/ic501695n | *Inorg. Chem.* 2014, 53, 12372−12377

bond dissociation is relatively fast in each case and that some other step is kinetically limiting. Similar secondary KIEs were previously observed for other nitrile hydration catalysts.[23,24] Further, the rate of hydration using *p*-chlorobenzonitrile substrate with precatalyst L^3RuPPh_3 is 2.5 times faster as compared to benzonitrile. This suggests the transition state is negatively charged, which is consistent with attack of water on metal-bound nitrile as the rate determining step.

Activation Parameters. To gain further insight into the reaction mechanism, nitrile hydration activation parameters for L^nRuPPh_3 (n = 1−3) were calculated by performing the reactions over a temperature range of 368−398 K. For each complex, a linear Arrhenius plot was obtained (see Supporting Information). A summary of experimentally determined values for L^nRuPPh_3 is provided in Table 2 with values for Co-NHase provided for comparison. As expected, L^1RuPPh_3 exhibits the largest activation energy barrier, 72.0 ± 14.0 kJ mol^{-1}, for the benzonitrile hydration. The activation barrier is similar in magnitude to that observed by Hirano et al. using a dipalladium catalyst.[23] Sulfur oxidation to the sulfinato complex L^2RuPPh_3 lowers the activation barrier by almost 27 kJ mol^{-1} to 45.3 ± 3.7 kJ mol^{-1}. Further S-oxidation to the sulfenato/sulfinato precatalyst L^3RuPPh_3 shows no statistical decrease in the hydration activation barrier. The same trend and magnitude of effect is observed in the enthalpy of activations ($\Delta H^{\ddagger}$).

Table 2. Nitrile Hydration Activation Parameters for L^nRuPPh_3 (n = 1−3) in DMF Determined over a Temperature Range 368−398 K and Co-NHase[25]

precatalyst	E_a (kJ mol^{-1})	$\Delta H^{\ddagger}$ (kJ mol^{-1})	$\Delta S^{\ddagger}$ (J K^{-1} mol^{-1})
L^1RuPPh_3	72.0 ± 14.0	68.9 ± 14.0	−67.8 ± 18.7
L^2RuPPh_3	45.3 ± 3.7	42.1 ± 3.7	−123.7 ± 15.3
L^3RuPPh_3	43.0 ± 8.3	39.8 ± 8.3	−123.2 ± 35.2
Co-NHase	23.0 ± 1.2	18.0 ± 0.9	−146.0 ± 0.7

The entropy of activation ($\Delta S^{\ddagger}$) sheds significant light on the effect of S-oxidation on the nature of the transition state. Sulfur oxidation nearly doubles $\Delta S^{\ddagger}$ from the parent complex L^1RuPPh_3 to the sulfinato complex L^2RuPPh_3 (Table 2). As with the enthalpic contribution, further S-oxidation to L^3RuPPh_3 results in no further statistically significant changes. These results indicate that molecular motions are substantially more restricted in the transition state of the S-oxidized catalysts. Interestingly, the $\Delta S^{\ddagger}$ values for L^2RuPPh_3 and L^3RuPPh_3 are statistically similar to those observed for Co-NHase.[25]

On the basis of these results we hypothesize that sulfur oxidation helps in the formation of an early transition state that leads to lower enthaplic barriers. This is consistent with DFT studies as discussed in more detail in the Computational Studies section. However, this imposes the significant entropy of activation observed for L^2RuPPh_3 and L^3RuPPh_3, and Co-NHase. However, this is more than offset by the substantial decrease in the enthalpy of activation upon S-oxidation. Notably, the enhanced Lewis acidity of the metal center upon S-oxidation, as noted in electrochemical studies (positive shift of half potential as result of sulfur oxidation) and XAS and DFT studies on L^nRuPPh_3,[19,26] is also expected to lower the enthalpic barrier. The further lowering of the enthalpy of activation of Co-NHase relative to L^2RuPPh_3 and L^3RuPPh_3 can be attributed to the greater Lewis of acidity of Co(III) as compared to Ru(II).

Computational Studies. To corroborate the experimental results, we employed a series of DFT studies using the B3LYP hybrid functional with the LanL2DZ basis set for Ru and 6-31G(d) for all other atoms.[27,28] All calculations were performed both in the gas phase and in DMF with consistent trends between the two series. Since the Fe(III) derivative of L^1RuPPh_3 was previously reported to bind nitrile, water, and amide in experimental studies,[29] we first evaluated the relative free energies of L^nRuPPh_3 (n = 1−3) with water, benzonitrile, and benzamide coordinated in place of PPh_3 (Table 3). For all three series, substrate binding is thermodynamically preferred over product or PPh_3 coordination consistent with the observed catalysis. Precatalysts L^1RuPPh_3 and L^2RuPPh_3 display a preference for water over benzonitrile with the oxidized L^2 ligand more strongly favoring water coordination. Further oxidation to L^3RuPPh_3 switches binding preference to nitrile consistent with the alternating effects of S-oxidation on nitrile binding affinity noted experimentally. Calculations in DMF show that each one of the ligands L^1, L^2, and L^3 favors nitrile binding over water where the nitrile coordination is much more pronounced for ligand L^3.

Table 3. Relative Free Energies (kJ/mol) for L^nRuPPh_3 (n = 1−3) upon Substitution of PPh_3 with H_2O, Benzonitrile (PhCN), and Benzamide ($PhC(O)NH_2$) from Gas Phase (and DMF) DFT Computations Using the B3LYP Hybrid Functional with the LanL2DZ Basis Set for Ru and 6-31G(d) for All Other Atoms

ligand	L^1RuPPh_3	L^2RuPPh_3	L^3RuPPh_3
PPh_3	0 (0)	0 (0)	0 (0)
H_2O	−29.4 (−33.3)	−45.8 (−49.5)	−30.7 (−30.4)
PhCN	−25.1 (−39.6)	−36.1 (−58.0)	−42.3 (−49.9)
$PhC(O)NH_2$	11.4 (5.0)	−13.1 (−4.6)	−10.3 (+1.9)

Given the relative energies of nitrile versus water binding for L^nRuPPh_3 (n = 1−3), we considered both nitrile-bound and water-bound catalytic hydration mechanisms. However, we could only locate a transition state for the former, using DFT, and the water-bound route was dismissed from further consideration. The calculated hydration mechanism involves nucleophilic attack of an associated water molecule on a metal-bound nitrile as the rate controlling step (Figure 3). The resulting iminol bound intermediate then rearranges to an N-bound amide product, which is readily displaced by water or nitrile completing the cycle.

The parent L^1RuNCR complex exhibits the largest enthalpic barrier in the gas phase (81.7 kJ/mol), which matches the experimentally measured barrier of 68.9 ± 14.0 kJ/mol. This barrier is significantly lower than the transition state enthalpy (203 kJ/mol) calculated for benzonitrile hydration in the absence of catalyst that serves as the blank reaction to compare the DFT calculated barriers. Oxidation to the sulfinato derivative L^2RuNCR reduces the enthalpic barrier by 21.7 kJ/mol to a barrier of 60.0 kJ/mol. The absolute decrease in calculated enthalpy matches the experimentally observed decrease of 26.8 kJ/mol remarkably well. Further S-oxidation to L^3RuNCR is predicted to lower the barrier by an additional 14.3 kJ/mol.

However, the anticipated decrease in the enthalpic barrier for L^3RuPPh_3 compared to L^2RuPPh_3 as suggested by DFT studies, as a result of sulfur oxidation to sulfenato, can neither

dx.doi.org/10.1021/ic501695n | Inorg. Chem. 2014, 53, 12372−12377

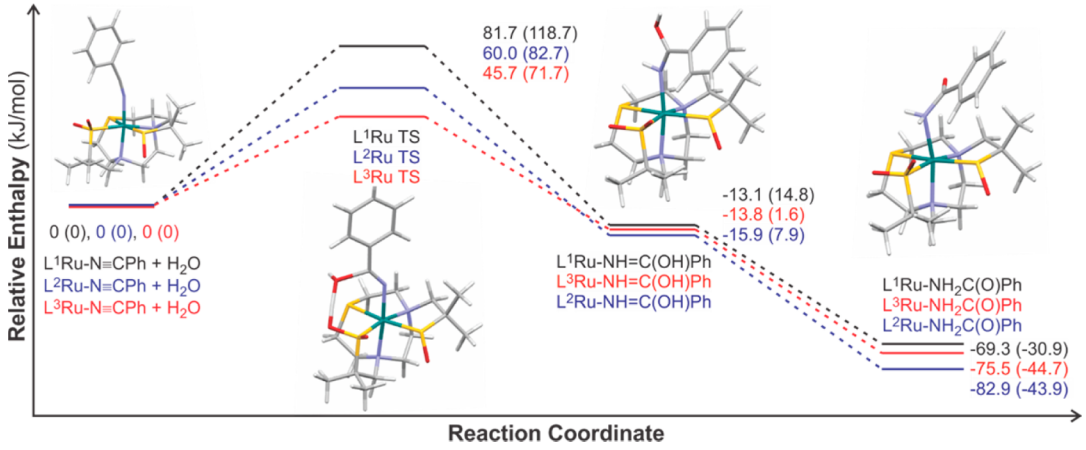

Figure 3. Calculated energetics of the nitrile-bound pathway for benzonitrile hydration for precatalysts L^1RuPPh_3 (black), L^2RuPPh_3 (blue), and L^3RuPPh_3 (red) using B3LYP hybrid functional and LanL2DZ basis set for Ru atom and 6-31G(d) for all other atoms under standard conditions (298 K). Enthalpies (kJ/mol) are given for gas phase and for DMF solvent phase in parentheses (TS = transition state).

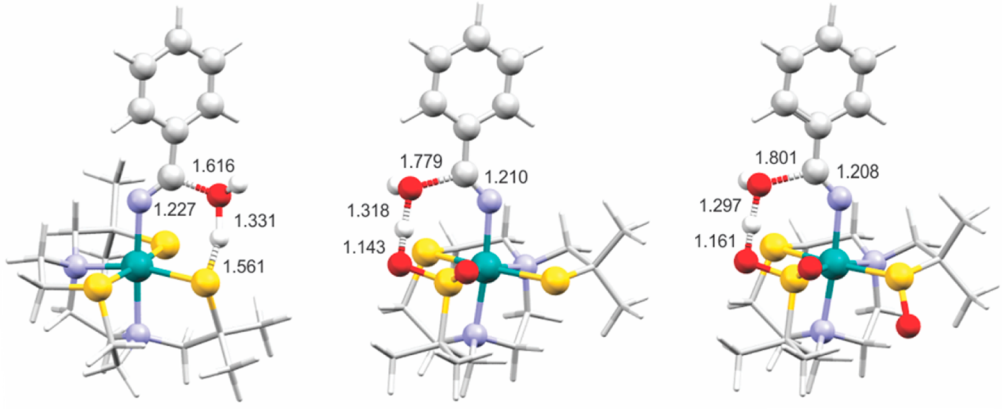

Figure 4. Gas phase transition state structures for L^nRuTS (n = 1−3).

be confirmed nor discounted due to experimental error associated with the experimentally determined barriers for precatalysts L^2RuPPh_3 and L^3RuPPh_3. Calculated activation enthalpies in DMF are higher than experimental results, but display the same trend upon S-oxidation. Further, our DFT results are consistent with prior reports by Himo and coworkers that note a reduction in the enthalpic barrier when sulfenate acts as a local base to activate water in NHase.[30]

Examination of transition structures for L^nRuTS (n = 1−3) confirms the high ordering foreshadowed by the entropic activation parameters (Figure 4). For all three catalysts, the Ru−N−C bond angle in the transition state structure is bent indicating substantial imidate character. The transition state of L^2RuPPh_3 displays a partial proton transfer from water to the sulfenato O with HO···H and SO···H distances of 1.318 and 1.143 Å, respectively. The corresponding distances in the transition state of L^3RuPPh_3 indicate slightly less transfer of the proton from the water. In L^1RuPPh_3, the proton is partially transferred to the thiolate donor with a slightly longer HO···H (1.331 Å) and a S···H distance of 1.561 Å. Taken together, these distances suggest lesser proton transfer is required in the transition state upon increased S-oxidation. All these observations indicate that an early transition state is observed for precatalyst with sulfur modification. An earlier transition state in the S-oxidized complexes is also indicated by the C−OH distance that increases from 1.616 to 1.779 to 1.801 Å from L^1RuPPh_3 to L^3RuPPh_3, with a corresponding decrease in the C−N distance due to additional triple bond character. The bond distance between Ru and N atom of nitrile ($Ru-N_{nitrile}$) is 2.068, 2.076, and 2.091 Å in transition state structures (gas phase) for L^1RuTS, L^2RuTS, and L^3RuTS, respectively. A similar elongation trend is observed for transitions states $L^{1-3}RuTS$ in the DMF phase. Elongation in $Ru-N_{nitrile}$ bond distance is also observed in the optimized nitrile-bound structures for $L^{1-3}RuNCPh$ in gas and DMF phase concomitant of sulfur oxidation. Therefore, it seems logical that early transition state formation for L^{2-3} is responsible for observed decrease in enthalpic barrier. The natural charges in the gas phase for $L^{1-3}RuNCPh$ suggest that sulfur oxidation enhances the polarization of the nitrile leading to formation of early transition state and decreased enthalpic barriers. A similar polarization trend is observed for natural charges calculated in the DMF phase. On the basis of the suggestion by an anonymous reviewer, we also investigated the Ru−OH catalyzed reaction for L^3RuPPh_3 precatalyst, but we were unable to locate a transition state for the metal-bound hydroxide reacting with the nitrile.

Relevance to Nitrile Hydratase. A proposed mechanism consistent with the kinetic data for L^nRuPPh_3 (n = 1−3) is detailed in Figure 5. The six-coordinate L^nRuPPh_3 precatalysts dissociate phosphine to give the inactive L^nRuOH_2 and active L^nRuNCR species in dynamic equilibrium. The latter under-

dx.doi.org/10.1021/ic501695n | Inorg. Chem. 2014, 53, 12372−12377

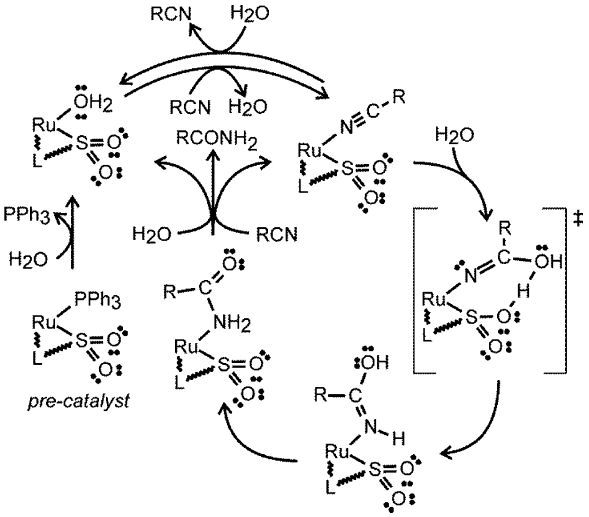

Figure 5. Proposed nitrile hydration catalytic cycle for L^{n}RuTS (n = 2−3; R = phenyl, L^n ligand abbreviated as L ~ SO_2 for clarity).

goes nucleophilic attack by water to form the highly ordered transition state complex. Rearrangement affords the N-bound iminol intermediate which tautomerizes to give the enthalpically preferred product complex L^{n}RuNH$_2$C(O)R. Substitution of amide by either the water or nitrile substrate completes the cycle.

Mechanistic proposals for NHase include both water-bound[9] and nitrile-bound pathways.[31−34] Our previous and current studies show a tendency for L^1 based ligand systems to bind both substrates in equilibrium.[29] Interestingly, S-oxidation to the sulfinate shifts binding in favor of water, whereas the mixed sulfenato/sulfinato donor set favors nitrile coordination. As the water-bound complex is catalytically impotent, the mixed sulfenato/sulfinato donor set most favors the kinetically competent intermediate. Interestingly, in NHase both the thiolate and sulfinato derivative are inactive, and only the mixed sulfenato/sulfinato donor set is catalytically active. This may be due, in part, to heightened affinity of nitrile over water for this S-oxidation state. However, by maintaining some binding affinity for water, NHase would be able to protect against undesirable metal-binding/activation of oxygen or other small molecules, while maintaining a reservoir of catalyst ready for activation upon the introduction of nitrile substrate.

Increased nitrile binding affinity is not the only advantage of the mixed sulfenato/sulfinato donor set. Sulfur oxidation enhances the polarization of the nitrile carbon, and that leads to attack of water through highly ordered organization of the transition state through H-bonding. Both our oxidized precatalysts (L^{2}RuPPh$_3$ and L^{3}RuPPh$_3$) and Co-NHase show a large and negative entropy of activation ($\Delta S^{\ddagger}$) of similar magnitude (Table 2). The enhanced polarization of the nitrile is reflected in the formation of early transition state and hence decreased enthalpic barrier for L^{2}RuPPh$_3$ and L^{3}RuPPh$_3$ relative to L^{1}RuPPh$_3$, which approach the barrier observed for Co-NHase (Table 2). *While such lowering of enthalpic barrier of the reaction has been long postulated, our series of complexes provided for the first experimental kinetic data to clearly demonstrate the anticipated enthalpic and entropic trends of S-oxidation on nitrile hydration.*

A significant difference between our complexes and the active site of NHase is the magnitude of effect observed upon S-oxidation. In our complexes, a *4-fold* increase in hydration rate is observed, whereas in NHase the catalyst goes from inactive to highly active after S-oxidation. One possible explanation is that Co(III) more strongly favors water coordination than our Ru(II) catalysts and that S-oxidation is mandatory for significant nitrile coordination in the latter. It should be noted that an alternate, ligand-centered nitrile hydration mechanism has been recently proposed for NHase on the basis of experimental and DFT studies in which the sulfenato (RSO^-) ligand serves as the active nucleophile.[34,35] While such a mechanism is inconsistent with the activity trends of L^{n}RuPPh$_3$ (n = 1−3), we are actively pursuing other model complexes to experimentally assess the validity of this mechanism.

■ CONCLUSIONS

In conclusion, the NHase inspired ruthenium(II) based precatalysts L^{n}RuPPh$_3$ (n = 1−3) provide a unique series of complexes to study the kinetic effect of S-oxidation on catalytic nitrile hydration. Through such studies, we show that S-oxidation increases the hydration rate 4-fold through enhanced nitrile binding and formation of early transition state due to greater nitrile polarization. We propose that both effects are responsible for the S-oxidation requirement in NHase for nitrile hydration activity. With our models, we have detailed for the first time substantial shifts in enthalpic and entropic parameters upon S-oxidation that promote nitrile hydration activity. Specifically, the entropic term approaches that observed for NHase supporting a highly organized transition state upon S-oxidation. The experimental findings are well correlated with the density functional theory results.

■ EXPERIMENTAL SECTION

Materials and Methods. All manipulations involving air- or moisture-sensitive compounds were carried out using standard Schlenk techniques under argon. Samples were stored in a glovebox under argon atmosphere. Benzonitrile was purchased from Alfa-Aesar while benzamide, *p*-tolunitrile, *p*-toluamide, and nuclease free water were all purchased from Sigma-Aldrich. The precatalysts L^{1}RuPPh$_3$, L^{2}RuPPh$_3$, and L^{3}RuPPh$_3$ were synthesized using the established protocols as reported earlier.[18,19] The purity of each complex was confirmed using square wave voltammetry.

Instrumentation. The GC−MS instrument used in the studies was obtained from Agilent Technologies augmented with 7820A GC system and 5975 series MSD using helium as a carrier gas at a flow rate of 1.00 mL/min. The oven and inlet temperature were set to and 180 and 300 °C, respectively. The column used was poly(5% diphenyl, 95% dimethylsiloxane) with length 30 m, 250 μm inner diameter, and 0.25 μm thickness. A split ratio of 20:1 was employed in the studies.

Computational Methodology. The DFT calculations were carried out at the B3LYP level of theory using 6-31G(d) basis set for C, H, N, S, O, and P atoms and LanL2DZ basis set for Ru atom with effective core potential. The initial coordinates for precatalyst L^{1}RuPPh$_3$ were obtained from the crystal structure, and for L^{2}RuPPh$_3$ and L^{3}RuPPh$_3$ coordinates were generated from L^{1}RuPPh$_3$ by addition of required number of oxygen atoms. The initial coordinates for derivatives of precatalyst L^{1}RuPPh$_3$ (benzonitrile/water at the place of PPh$_3$ etc.) were obtained by substituting the phosphine with the corresponding group, and then it was optimized. Similar methodology was undertaken for derivatives of precatalyst L^{2}RuPPh$_3$ and L^{3}RuPPh$_3$. The optimized coordinates are listed for all the compounds. The calculations were carried out in gas phase as well as in solution phase, using *N*,*N*′-dimethylformamide (DMF) solvent. The polarity effect of bulk solvent was evaluated by the conductor-like polarized continuum model (CPCM) at the same level of theory. The frequency calculations were performed at the aforementioned level of theory to identify the nature of all stationary points, and the transition states

dx.doi.org/10.1021/ic501695n | *Inorg. Chem.* 2014, 53, 12372−12377

were identified as the ones with only single negative frequency. All the reported enthalpies and free energies of reactions have been corrected for zero-point energies. All quantum-chemical calculations were performed with *Gaussian09* program package.[36] The Chemcraft software was utilized for visualization. The natural population analysis was performed using NBO program included in the Gaussian 09.[37]

Typical Procedure for Kinetic Studies. The reactions were carried out in an 8 mL glass vial, open top closure sealed with PTFE septa, equipped with a magnetic stir bar. A typical run included 500 μL of catalyst stock solution in DMF, 500 μL of benzonitrile, 500 μL of H_2O, and 1000 μL of DMF solvent, keeping a total volume of 2.500 mL. The samples were prepared under inert conditions and were placed in an oil bath at 398 K. The concentration of catalyst was changed using different volumes of stock solution, and similarly, PhCN and H_2O concentrations were varied. The volume of DMF was adjusted to keep the total reaction volume 2.500 mL. The aliquots were removed periodically depending upon the catalyst, then internal standard was added to the aliquots, and the samples were subjected to GC−MS analysis.

■ ASSOCIATED CONTENT

Ⓢ Supporting Information

Kinetic traces for $L^{1-3}RuPPh_3$, rate law derivation, and optimized coordinates from density functional theory studies for $L^{1-3}Ru$ and $L^{1-3}RuX$ (X = PPh_3, PhCN, H_2O, $PhCONH_2$, PhC(OH)NH, and TS) in gas and DMF solvent phase. The material is available free of charge from via the Internet at http://pubs.acs.org.

■ AUTHOR INFORMATION

Corresponding Author

*E-mail: grapperhaus@louisville.edu. Fax: +1 502 852-8149. Phone: +1 502 852-5932.

Notes

The authors declare no competing financial interest.

■ ACKNOWLEDGMENTS

We acknowledge the National Science Foundation (CHE-0749965) for funding and a Competitive Enhancement Grant from the Office of the Executive Vice President for Research and Innovation (University of Louisville) for continued support. The authors are thankful to Cardinal Research Cluster at the University of Louisville for providing the computational facilities.

■ REFERENCES

(1) Murakami, T.; Nojiri, M.; Nakayama, H.; Odaka, M.; Yohda, M.; Dohmae, N.; Takio, K.; Nagamune, T.; Endo, I. *Protein Sci.* **2000**, *9*, 1024.
(2) Kovacs, J. A. *Chem. Rev.* **2004**, *104*, 825.
(3) Harrop, T. C.; Mascharak, P. K. *Acc. Chem. Res.* **2004**, *37*, 253.
(4) Yano, T.; Ozawa, T.; Masuda, H. *Chem. Lett.* **2008**, *37*, 672.
(5) Prasad, S.; Bhalla, T. C. *Biotechnol. Adv.* **2010**, *28*, 725.
(6) Shearer, J.; Callan, P. E.; Amie, J. *Inorg. Chem.* **2010**, *49*, 9064.
(7) O'Toole, M. G.; Kreso, M.; Kozlowski, P. M.; Mashuta, M. S.; Grapperhaus, C. A. *J. Biol. Inorg. Chem.* **2008**, *13*, 1219.
(8) Kung, I.; Schweitzer, D.; Shearer, J.; Taylor, W. D.; Jackson, H. L.; Lovell, S.; Kovacs, J. A. *J. Am. Chem. Soc.* **2000**, *122*, 8299.
(9) Tyler, L. A.; Noveron, J. C.; Olmstead, M. M.; Mascharak, P. K. *Inorg. Chem.* **2003**, *42*, 5751.
(10) Bourles, E.; Alves de Sousa, R.; Galardon, E.; Giorgi, M.; Artaud, I. *Angew. Chem.* **2005**, *117*, 6318.
(11) Galardon, E.; Giorgi, M.; Artaud, I. *Chem. Commun.* **2004**, 286.
(12) Lugo-Mas, P.; Dey, A.; Xu, L.; Davin, S. D.; Benedict, J.; Kaminsky, W.; Hodgson, K. O.; Hedman, B.; Solomon, E. I.; Kovacs, J. A. *J. Am. Chem. Soc.* **2006**, *128*, 11211.
(13) Yano, T.; Arii, H.; Yamaguchi, S.; Funahashi, Y.; Jitsukawa, K.; Ozawa, T.; Masuda, H. *Eur. J. Inorg. Chem.* **2006**, *2006*, 3753.
(14) Yano, T.; Wasada-Tsutsui, Y.; Arii, H.; Yamaguchi, S.; Funahashi, Y.; Ozawa, T.; Masuda, H. *Inorg. Chem.* **2007**, *46*, 10345.
(15) Rose, M. J.; Betterley, N. M.; Mascharak, P. K. *J. Am. Chem. Soc.* **2009**, *131*, 8340.
(16) Heinrich, L.; Mary-Verla, A.; Li, Y.; Vaissermann, J.; Chottard, J. C. *Eur. J. Inorg. Chem.* **2001**, *2001*, 2203.
(17) Rat, M.; Sousa, R. A. d.; Tomas, A.; Frapart, Y.; Tuchagues, J.-P.; Artaud, I. *Eur. J. Inorg. Chem.* **2003**, *2003*, 759.
(18) Masitas, C. A.; Mashuta, M. S.; Grapperhaus, C. A. *Inorg. Chem.* **2010**, *49*, 5344.
(19) Masitas, C. A.; Kumar, M.; Mashuta, M. S.; Kozlowski, P. M.; Grapperhaus, C. A. *Inorg. Chem.* **2010**, *49*, 10875.
(20) Grapperhaus, C. A.; Patra, A. K.; Mashuta, M. S. *Inorg. Chem.* **2002**, *41*, 1039.
(21) Shigehiro, S.; Nakasako, M.; Dohmae, N.; Tsujimura, M.; Tokoi, K.; Odaka, M.; Yohda, M.; Kamiya, N.; Endo, I. *Nat. Struct. Biol.* **1998**, *5*, 347.
(22) Kumar, D.; Masitas, C. A.; Nguyen, T. N.; Grapperhaus, C. A. *Chem. Commun.* **2013**, *49*, 294.
(23) Hirano, T.; Uehara, K.; Kamata, K.; Mizuno, N. *J. Am. Chem. Soc.* **2012**, *134*, 6425.
(24) Shimizu, K.-i.; Kubo, T.; Satsuma, A.; Kamachi, T.; Yoshizawa, K. *ACS Catal.* **2012**, *2*, 2467.
(25) Mitra, S.; Holz, R. C. *J. Biol. Chem.* **2007**, *282*, 7397.
(26) Shearer, J.; Callan, P. E.; Masitas, C. A.; Grapperhaus, C. A. *Inorg. Chem.* **2012**, *51*, 6032.
(27) Becke, A. D. *J. Chem. Phys.* **1993**, *98*, 1372.
(28) Hay, P. J.; Wadt, W. R. *J. Chem. Phys.* **1985**, *82*, 270.
(29) O'Toole, M. G.; Bennett, B.; Mashuta, M. S.; Grapperhaus, C. A. *Inorg. Chem.* **2009**, *48*, 2300.
(30) Hopmann, K. H.; Himo, F. *Eur. J. Inorg. Chem.* **2008**, *2008*, 1406.
(31) Swartz, R. D.; Coggins, M. K.; Kaminsky, W.; Kovacs, J. A. *J. Am. Chem. Soc.* **2011**, *133*, 3954.
(32) Hashimoto, K.; Suzuki, H.; Taniguchi, K.; Noguchi, T.; Yohda, M.; Odaka, M. *J. Biol. Chem.* **2008**, *283*, 36617.
(33) Gumataotao, N.; Kuhn, M. L.; Hajnas, N.; Holz, R. C. *J. Biol. Chem.* **2013**, *288*, 15532.
(34) Hopmann, K. H. *Inorg. Chem.* **2014**, *53*, 2760.
(35) Martinez, S.; Wu, R.; Sanishvili, R.; Liu, D.; Holz, R. *J. Am. Chem. Soc.* **2014**, *136*, 1186.
(36) Frisch, M. J.; Trucks, G. W.; Schlegel, H. B.; Scuseria, G. E.; Robb, M. A.; Cheeseman, J. R.; Scalmani, G.; Barone, V.; Mennucci, B.; Petersson, G. A.; Nakatsuji, H.; Caricato, M.; Li, X.; Hratchian, H. P.; Izmaylov, A. F.; Bloino, J.; Zheng, G.; Sonnenberg, J. L.; Hada, M.; Ehara, M.; Toyota, K.; Fukuda, R.; Hasegawa, J.; Ishida, M.; Nakajima, T.; Honda, Y.; Kitao, O.; Nakai, H.; Vreven, T.; Montgomery, J. A., Jr.; Peralta, J. E.; Ogliaro, F.; Bearpark, M.; Heyd, J. J.; Brothers, E.; Kudin, K. N.; Staroverov, V. N.; Kobayashi, R.; Normand, J.; Raghavachari, K.; Rendell, A.; Burant, J. C.; Iyengar, S. S.; Tomasi, J.; Cossi, M.; Rega, N.; Millam, N. J.; Klene, M.; Knox, J. E.; Cross, J. B.; Bakken, V.; Adamo, C.; Jaramillo, J.; Gomperts, R.; Stratmann, R. E.; Yazyev, O.; Austin, A. J.; Cammi, R.; Pomelli, C.; Ochterski, J. W.; Martin, R. L.; Morokuma, K.; Zakrzewski, V. G.; Voth, G. A.; Salvador, P.; Dannenberg, J. J.; Dapprich, S.; Daniels, A. D.; Farkas, Ö.; Foresman, J. B.; Ortiz, J. V.; Cioslowski, J.; Fox, D. J. *Gaussian09*; Gaussian, Inc.: Wallingford, CT, 2009.
(37) Glendening, E. D.; Reed, A. E.; Carpenter, J. E.; Weinhold, F. *NBO Version 3.1*.